RSC Advances

PAPER

View Article Online
View Journal | View Issue

Cite this: *RSC Adv.*, 2024, **14**, 3567

Efficient removal of tetracycline in water using modified eggplant straw biochar supported green nanoscale zerovalent iron: synthesis, removal performance, and mechanism†

Guofu Huang,[abc] Mianmian Wang, *[abc] Qing Liu,[abc] Shasha Zhao,[abc] Haijian Liu,[abc] Fangfang Liu[ab] and Jun Liu[ab]

Received 9th December 2023
Accepted 16th January 2024

DOI: 10.1039/d3ra08417e

rsc.li/rsc-advances

A novel NaOH modified eggplant straw biochar supported green nanoscale zerovalent iron (P-nZVI/ESBC) composite was synthesized and its removal performance and reaction mechanism for tetracycline (TC) in water were investigated. Multiple characterizations showed that the prepared P-nZVI/ESBC composite contained oxygen-containing functional groups (hydroxyl, carbonyl, and carboxyl groups) and Fe species (nZVI and its oxides). The dosage of composite, temperature, and solution pH significantly affected the removal capacity of the P-nZVI/ESBC composite for TC. The Avrami fraction-order kinetic model and Sips adsorption isotherm model can fit well the removal process of TC by the P-nZVI/ESBC composite, indicating that the adsorption behavior of TC involved multiple adsorption mechanisms and chemical adsorption might occur. The maximum adsorption capacity of the P-nZVI/ESBC composite for TC was 304.62 mg g^{-1}. The adsorption and reductive degradation were the dominant mechanisms of TC removal by the P-nZVI/ESBC composite. This work offers abundant information on the application of eggplant straw to manufacture biochar-based composites for the efficient removal of antibiotic contaminants from aquatic environments.

1. Introduction

Tetracycline (TC), an important antibiotic, is widely used in human medicine, livestock and poultry industry because of its excellent antibacterial properties and low price.[1,2] It was previously reported that about 60–90% of TC was excreted into the environment in the form of parent compound and its incomplete metabolic products *via* urine and feces,[3] and the total emissions are increasing year by year.[4] TC has high water solubility; a large fraction of discharged TC ends up in water bodies, sediment and soil.[5] The misuse and improper disposal of antibiotics would lead to an increase in microbial resistance, exacerbating the abundance and diversity of antibiotic resistance genes and antibiotic resistant bacteria in the environment, and potentially threatening human health and ecological security.[6,7] Therefore, it is urgent to reduce the amount of residual TC in nature, especially in water.

Nowadays, some techniques have been developed to eliminate antibiotics, including adsorption,[1,3,8] membrane separation,[9] biodegradation,[10] catalytic reduction,[5,11] photocatalysis,[12,13] and advanced oxidation processes.[14–16] Among these techniques, adsorption and degradation methods are well accepted due to their high removal efficiency, flexibility, and low-price. Biochar is a carbon-rich solid product produced by the thermochemical process from raw materials containing biomass. Related studies showed that biochar, with its large specific surface area and abundant functional groups, could be widely employed to remove the pollutants in the environment.[1,8,17,18] Generally, biochar was prepared by hydrothermal carbonization and pyrolysis routes.[2,19,20] Compared to pyrolysis route (400–800 °C), hydrothermal carbonization can yield more biochar solids at mild temperature (180–350 °C), and the fresh raw materials do not require further drying treatment.[19–21] However, these biochar materials generally have relatively small specific surface areas and poor pore structures,[17] resulting in the limited adsorption performance for pollutants. Alkali activation can effectively enhance the specific surface areas of biochar, change the surface charge, and increase the surface oxygen-containing functional groups, thus improving the adsorption performance for pollutants.[17,18] Agricultural and forestry wastes are rich in biomasses, which are ideal raw materials of biochar production. Eggplant, an important

[a]School of Chemical Engineering and Environment, Weifang University of Science and Technology, Weifang, 262700, China. E-mail: 253463877@qq.com
[b]Shandong Engineering Laboratory for Clean Utilization of Chemical Resources, Weifang, 262700, China
[c]Weifang Key Laboratory of Chemical Wastewater Pollution Control and Resource Reuse, Weifang, 262700, China

† Electronic supplementary information (ESI) available. See DOI: https://doi.org/10.1039/d3ra08417e

vegetable, is widely planted in China. Most of eggplant straws, accompanying products of eggplant cultivation, were discarded or burned directly as fuel, which would cause a waste of resource and pollute the surrounding environment. Therefore, in the study, eggplant straws were used as the raw materials and sodium hydroxide (NaOH) as the activator to prepare modified biochar (ESBC) by hydrothermal carbonization route.

Nanoscale zero-valent iron (nZVI) has a large specific surface area, excellent reducing property and environmental friendliness. Consequently, it is often used as an excellent catalyst and adsorbent to remove various contaminants, including antibiotics.[22–24] However, nZVI is prone to agglomeration and oxidation due to its strong magnetic force, high surface energy, and strong reducing activity,[23] which limits its large-scale application in environmental remediation. Anchoring nZVI onto biochar can not only disperse nZVI well and prevent agglomeration, but also enhance the electron migration of nZVI and retard the oxidation of nZVI.[2] The combination of dispersed nZVI and modified biochar may improve the removal performance for TC in water. In addition, most of iron-based composites were synthesized by potassium/sodium borohydride reduction.[24,25] However, borohydride reagents are toxic and the synthesis process produces large amounts of inflammable hydrogen gas. Alternatively, the green synthesis method using plant extracts has received much attention due to its efficiency, convenience and environmental friendliness. Studies[26–29] showed that plant extracts (such as tea, eucalyptus leaves, and citrus peels) were rich in polyphenols and flavonoids, which can act as the reducing and capping agents to prepare iron-based composite. Pomegranate peel, a by-product of pomegranate cultivation, is also rich in bioactive substances such as polyphenols, flavonoids, and organic acids. However, by far, there are limited studies on the preparation of the composite of green nZVI immobilized on alkali-modified biochar using pomegranate peel extract as a green reducing agent. The removal performance and reaction mechanism of TC from aqueous solutions by the composite are not unclear.

In this study, a novel P-nZVI/ESBC composite was prepared using pomegranate peel extract as the green reducing agent and ESBC as the carrier. The physical and chemical property of P-nZVI/ESBC composite was characterized using SEM, BET, XRD, FTIR, and XPS methods. Besides, batch experiments were performed to investigate the effects of various influencing factors (including various prepared materials, P-nZVI/ESBC dosage, initial pH of TC solution, and reaction temperature) on TC removal. Finally, the adsorption kinetics, adsorption isotherms, and removal mechanism of TC with P-nZVI/ESBC composite were studied.

2. Materials and methods

2.1. Materials

Tetracycline hydrochloride ($C_{22}H_{24}N_2O_8 \cdot HCl$, ≥98.0%), $FeSO_4 \cdot 7H_2O$ (≥99.0%), and $NaBH_4$ (≥98.0%) were obtained from Aladdin Shanghai, China. Anhydrous ethanol (CH_3CH_2OH, ≥99.5%), NaOH (≥97.0%), H_2SO_4 (≥98.0%), and HCl (>37%) were purchased from Sinopharm Shanghai, China. All above reagents were analytically pure and were used directly without further treatment. The eggplant straws were collected from the vegetable base in Shouguang, China. Prior to the experiment, deionized water was purified with N_2 for 30 min to obtain deoxygenated water.

2.2. Preparation and characterization of various materials

Eggplant straw-derived biochar (ESBC) was prepared by modified hydrothermal carbonization method.[21] Briefly, ESBC was prepared by adding 5 g of eggplant straw powders and 50 mL of NaOH aqueous solution (100 g L^{-1}) to an autoclave reactor with Teflon lining. Then, the autoclave reactor was heated to 250 °C and maintained for 2 h under autogenic pressure and oxygen-limited conditions. The yielded solids were soaked in 1 mol L^{-1} of HCl solution for 4 h to remove excess impurities and washed thoroughly with deionized water, and then dried at 105 °C for further use.

The pomegranate peel extracts (50 g L^{-1}) were obtained by heating dried pomegranate peel powers in deionized water at 80 °C for 2 h and vacuum filtrated for further use. P-nZVI/ESBC composite was synthesized by the following liquid phase reduction method using pomegranate peel extract as green reducing agent. Typically, 0.5 g of ESBC and 0.8297 g of $FeSO_4 \cdot 7H_2O$ were added to a 250 mL of three-necked flask containing 100 mL of deoxygenated water, and stirred thoroughly for 2 h at room temperature. Then, 50 mL of pomegranate peel extracts were added dropwise to the mixed solution and stirred for another 1 h. In this process, Fe^{2+} was reduced to nZVI and immobilized onto ESBC to form P-nZVI/ESBC composite. The above reactions were carried out under nitrogen protection. The formed solid composite was collected by centrifugation and washed three times with deoxygenated water and anhydrous ethanol, respectively. Finally, P-nZVI/ESBC composite was vacuum dried at 80 °C for 12 h for further use. As a comparison, P-nZVI was prepared by the same method without the addition of ESBC. Meanwhile, B-nZVI/ESBC composite was also prepared using $NaBH_4$ as the reducing agent in the Text S1 (ESI).†

The physical and chemical properties of the as-synthesized materials were characterized by SEM, BET, XRD, FTIR, XPS and zeta potential methods, as shown in the Text S2 (ESI).†

2.3. Batch experiments

The typical effecting factor experiments of TC removal were conducted in 250 mL of sealed flasks under nitrogen atmosphere. In a typical run, 0.1 g of prepared material was added into flasks containing 100 mL of TC solution (50 mg L^{-1}), then the mixture in the flask was shaken at 180 rpm. At the given time intervals, 2 mL of samples were taken with glass syringes and passed through 0.22 μm membrane filters to analyze the residual concentration of TC in aqueous solution. To study the effect of pH, the initial pH of TC solution was adjusted to 3.0, 6.0, 9.0, and 11.0 using 0.1 mol per L H_2SO_4 and NaOH solutions. All experiments were carried out in triplicate.

The adsorption kinetics experiments were conducted in a series of 250 mL flasks containing 0.1 g of prepared P-nZVI/

ESBC composite and 100 mL of TC solution (50 mg L^{-1} and 300 mg L^{-1}, respectively). These flasks were shaken at 180 rpm for 4 h. At given time intervals, samples were collected and filtered and determined the concentration of TC. The adsorption isotherms studies were performed at different initial concentrations of TC (50–400 mg L^{-1}). Based on the adsorption kinetics studies, the equilibrium time was set to 4 h.

To examine the regeneration property of the material, the used P-nZVI/ESBC composites were immersed in NaOH solution (0.1 mol L^{-1}) and ultrasonically shaken for 12 h at ambient temperature. Then, the regenerative materials were washed, vacuum dried and used for the next recycling experiment.

In this study, the removal rates of TC in aqueous solution by various materials were obtained by the eqn (1):

$$\text{Removal rate}(R,\%) = \frac{C_0 - C_t}{C_0} \times 100\% \quad (1)$$

The adsorption amount of TC by P-nZVI/ESBC composite was calculated as:

$$q_t = \frac{(C_0 - C_t)V}{m} \quad (2)$$

$$q_e = \frac{(C_0 - C_e)V}{m} \quad (3)$$

where, R (%) relates to the removal rate of TC; C_0 (mg L^{-1}) and C_t (mg L^{-1}) associate with the initial and residual TC concentrations at reaction time t (min); q_t (mg g^{-1}) and q_e (mg g^{-1}) are the adsorbed quantity of TC at any time t (min) and the equilibrium time (min), respectively; C_e (mg L^{-1}) stands for the equilibrium concentration of TC; V (mL) represents the volume of reaction solution and m (g) is the mass of material.

2.4. Analytical procedures

The residual concentration of TC in aqueous solution was measured by an UV-vis spectrophotometer (TU-1950, Beijing General, China) at 355 nm. The pH and oxidation–reduction potential (ORP) of the solution were measured with a pH meter (Mettler, FE 28, China). Total Organic Carbon (TOC) in aqueous solutions was measured using a TOC analyzer (TOC-L, Shimadzu, Japan). The possible degradation products of TC were measured using an UPLC-QTOF-HRMS (Xevo-G2-XS, Waters, USA) equipment with electron spray ionization (ESI) in the negative ion mode. The mobile phase was composed of 45% formic acid (0.01 mol L^{-1}), 35% acetonitrile, and 20% methanol. The flow rate was set to 0.2 mL min^{-1}. An ACQUITY UPLC BEH C18 Column (1.7 μm, 2.1 mm × 100 mm, Waters, USA) was used. The pH of all samples was adjusted to 6.0 using 0.1 mol per L H_2SO_4 and NaOH solutions prior to measurement.

3. Results and discussion

3.1. Characterization of prepared materials

The microstructures of prepared ESBC and P-nZVI/ESBC composites are shown in Fig. 1. ESBC has rough surfaces with abundant porous channels (Fig. 1A), which provides large specific surface area. Fig. 1B shows that near-spherical nZVI particles with the size of about 40–120 nm (Fig. S1 in the ESI†) were successfully synthesized and immobilized on ESBC surfaces, which was helpful to inhibit the agglomeration of nZVI.[2] The EDS element mapping spectra of P-nZVI/ESBC composite (Fig. 1C) reveal that Fe was uniformly distributed on the composite surface. The surface area, pore volume and pore size of P-nZVI/ESBC composite are shown in Fig. S2 and Table S1 (ESI).† The N_2 isotherm obtained was typical type IV with H4 hysteresis loop, indicating the presence of mesoporous structures.[17,18] The calculated BET surface area of P-nZVI/ESBC composite was 203.81 m^2 g^{-1}, which may be attributed to the activation of NaOH during the hydrothermal process.

The crystalline structures of ESBC and P-nZVI/ESBC composites are shown in Fig. 2A. For ESBC, the apparent broad peak at about 2θ = 20–25° in XRD pattern was observed, corresponding to the amorphous carbon.[14,30] Compared with ESBC, the XRD spectrum of P-nZVI/ESBC composite exhibited weak α-Fe^0 characteristic peaks at 2θ of 44.6° and 65.2° (JCPDS #06-0696),[14] indicating that nZVI was successfully immobilized on the surfaces of ESBC. However, the intensity of α-Fe^0 reflection on the diffractogram appears quite weak, which may be attributed to organic materials from pomegranate peel extract encapsulated on the surfaces of nZVI.[26,31] Similar result was found in the XRD spectrum of P-nZVI (Fig. S3 in the ESI†). Additional, for P-nZVI and P-nZVI/ESBC composite, no obvious iron oxidation peaks were observed, which may be attributed to the positive protection of pomegranate peel extract.[32]

Fig. 2B shows the FTIR spectra of pomegranate peel extract, ESBC, and P-nZVI/ESBC composite. For pomegranate peel extract, the broad peak between 3600 and 3300 cm^{-1} indicates the existence of –OH functional group derived from polyphenol compounds.[33] Polyphenols played an important role in the reduction preparation and stabilization of nZVI.[27,34] For the case of ESBC, the peaks at about 3413, 2926, 1621, 1514, and 801 cm^{-1} are associated with –OH, aliphatic $-CH_2$, aromatic C=C/C=O, aromatic C–O, and aromatic C–H,[14,19,30,35] respectively. Two peaks at 1060 and 1025 cm^{-1} correspond to C–O stretching vibration.[19] The above results indicate that ESBC is rich in oxygen-containing functional groups (such as hydroxyl, carbonyl, and carboxyl groups) and that aromatic structures are formed during the hydrothermal reaction. In addition, compared with ESBC, the peak at around 1702 cm^{-1} of P-nZVI/ESBC composite associates with C=O stretching vibration,[19,20] which may be contributed to the oxidation of phenolic hydroxyl groups (–OH) of pomegranate peel extract.[33] The new weak peak at 565 cm^{-1} is related to the Fe–O band,[30,31] indicating the presence of Fe oxides on the surface of P-nZVI/ESBC composite. These oxides might be a result of nZVI oxidation.

The chemical structures of prepared materials were further analyzed by XPS, as shown in Fig. 3. In the full-range survey spectra of ESBC and P-nZVI/ESBC composite (Fig. 3A), obvious C 1s, O 1s, and N 1s peaks are observed. In addition, for P-nZVI/ESBC composite (Fig. 3A), Fe 2p peaks are found, indicating the presence of Fe species on the surfaces of synthesized materials. In the high-resolution Fe 2p spectrum of P-nZVI/ESBC composite (Fig. 3B), the peaks located at binding energies of

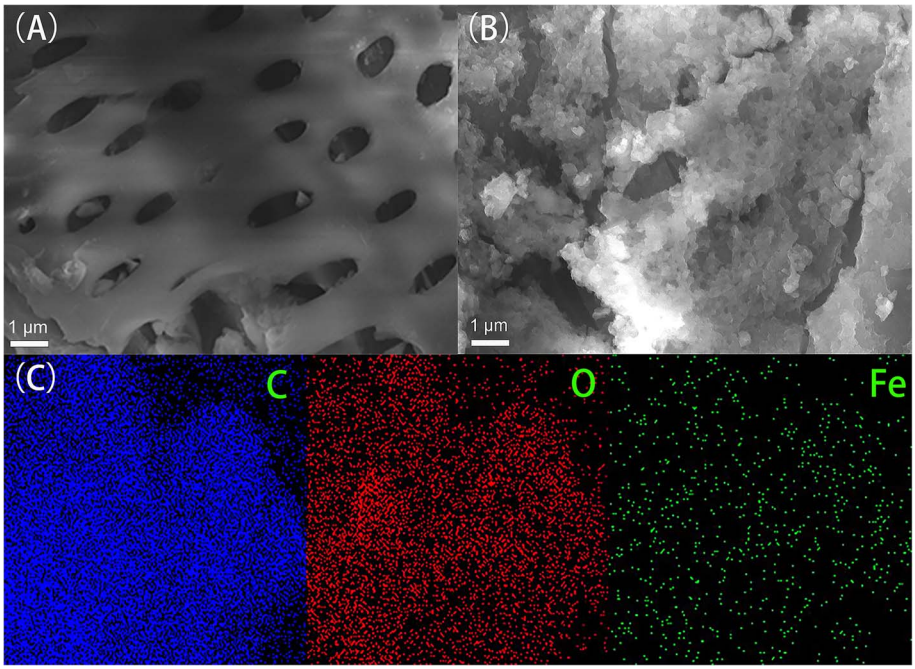

Fig. 1 SEM images of ESBC (A) and P-nZVI/ESBC composite (B), EDS mapping of P-nZVI/ESBC composite (C).

near 706.4 eV, 711.6 eV, and 725.1 eV represent Fe $2p_{3/2}$, Fe $2p_{3/2}$, and Fe $2p_{1/2}$, respectively. The fitted peak near 706.4 eV (Fe $2p_{3/2}$) can be observed, which corresponds to the typical zero-valent iron (Fe^0), showing the generation of Fe^0 on the surface of P-nZVI/ESBC composite. The fitted peaks at about 710.9 eV (Fe $2p_{3/2}$), 713.5 eV (Fe $2p_{3/2}$), and 716.8 eV (Fe $2p_{3/2}$) correspond to Fe^{2+} and Fe^{3+} oxide species,[36] which may be ascribed to the partial oxidation of nZVI on the composite surfaces during preparation and preservation. In Fig. 3C, the C 1s spectrum of P-nZVI/ESBC composite can be decomposed into four peaks at around 284.1 eV, 284.8 eV, 286.1 eV, and 288.3 eV, corresponding to C in C=C (aromatic carbon), C–OH, C–O–C, and O–C=O,[30,36] respectively. Similarly, the O 1s spectrum can be fitted into three individual peaks at around 530.3 eV, 531.4 eV, and 532.1 eV, which are associated with Fe–O (lattice oxide oxygen), C–O, and C=O,[30,36] respectively. In summary, these results suggest that the prepared P-nZVI/ESBC composite contain oxygen-containing functional groups (hydroxyl, carbonyl, and carboxyl groups) and Fe species (zero-valent iron and its oxides).

3.2. Effect of different experimental conditions on TC removal

3.2.1. Effect of different prepared materials. The removal of TC in aqueous solution with ESBC, P-nZVI, B-nZVI/ESBC, and P-nZVI/ESBC composites are shown in Fig. 4A. It is evident that the removal performance of as-synthesized materials for TC follows the following order: P-nZVI/ESBC > B-nZVI/ESBC > ESBC > P-nZVI. For P-nZVI, 46.4% of TC in aqueous solution was removed within 240 min, which was attributed to the adsorption and reductive degradation of nZVI.[22] According to the above SEM (Fig. 1A) and FTIR (Fig. 2B) analyses, ESBC possesses

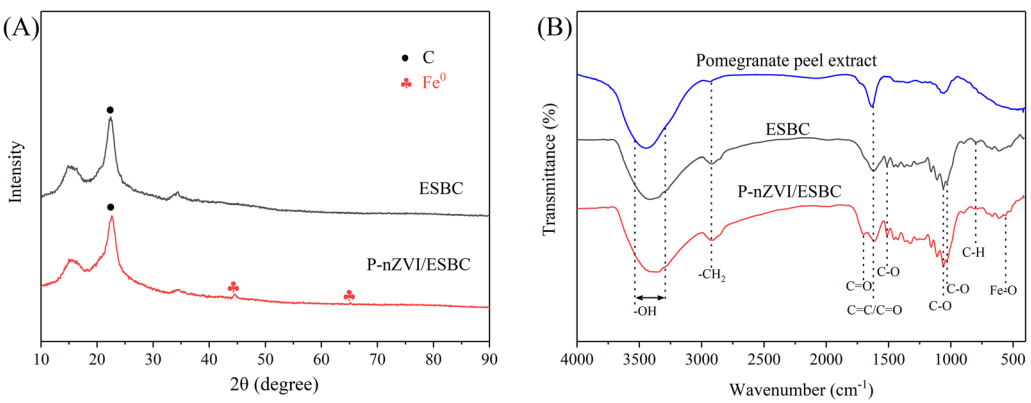

Fig. 2 XRD patterns (A) and FTIR spectra (B) of prepared materials.

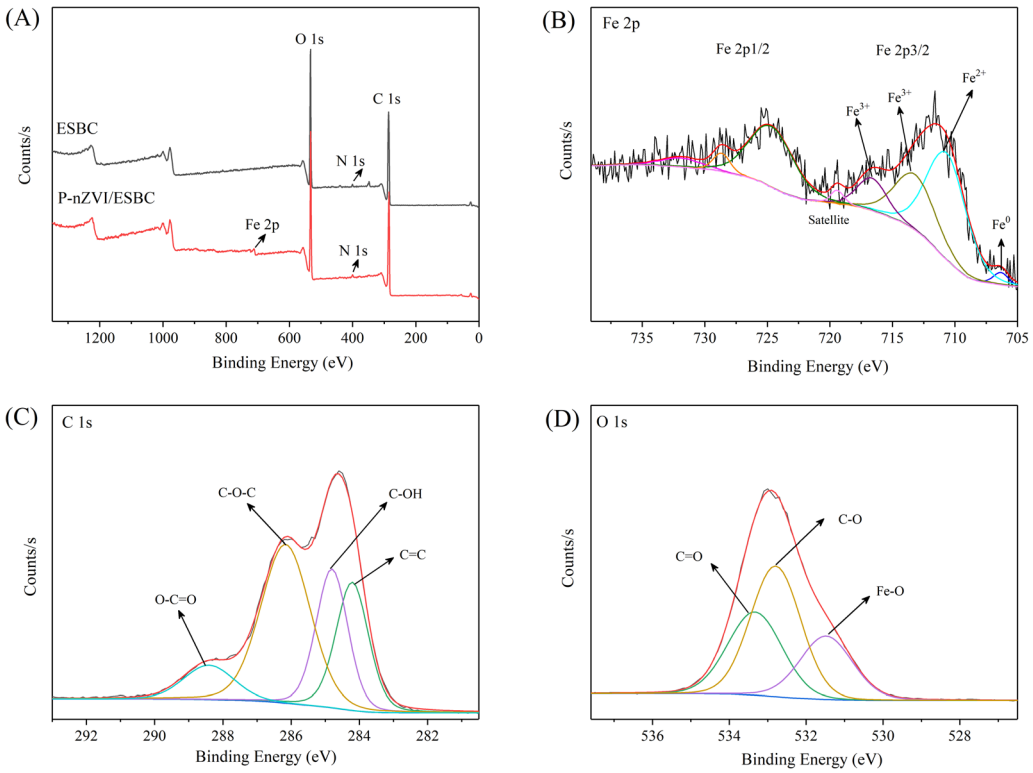

Fig. 3 The full-scan XPS spectra of ESBC and P-nZVI/ESBC composite (A), the high-resolution spectra of P-nZVI/ESBC composite: Fe 2p (B), C 1s (C), and O 1s (D).

abundant pores and oxygen-containing functional groups (hydroxyl, carbonyl, and carboxyl groups). Therefore, ESBC alone showed fine removal ability for TC, the removal rate reached 81.8% within 240 min. In the presence of B-nZVI/ESBC composite, around 88.4% of TC vanished in aqueous solution at 240 min. Compared to P-nZVI, ESBC, and B-nZVI/ESBC composite, P-nZVI/ESBC composite exhibited the best removal performance for TC, up to 98.0% of TC was removed at 240 min. These results could be illustrated by the following reasons: (i) as an excellent adsorbent and support material, biochar itself can not only adsorb TC, but also effectively disperse nZVI to provide more available active sites, thus promoting TC removal from aqueous solutions. (ii) Compared with the chemical reducing agent $NaBH_4$, P-nZVI/ESBC composite synthesized using pomegranate peel extract as reducing agent and capping agent can more effectively disperse nZVI particles and inhibit the oxidation of Fe^0.

3.2.2. Effect of P-nZVI/ESBC composite dosage. The effect of P-nZVI/ESBC composite dosage on the removal of TC in aqueous solution was investigated, as shown in Fig. 4B. It is clear that the removal rate of TC increases with increasing dose of P-nZVI/ESBC composite. When the dosage of P-nZVI/ESBC composite was 0.25 g L^{-1}, only 32.2% of TC (50 mg L^{-1}) was removed within 240 min. With the increase of P-nZVI/ESBC composite dosage from 0.5 g L^{-1} to 1.0 g L^{-1}, the corresponding removal rates of TC increased from 71.2% to 98.0%. The reasonable explanation is that the increased dosage of composite can provide more available active sites.[22,37] However, when the dosage of P-nZVI/ESBC composite further increased to 2.0 g L^{-1}, TC removal rate increased only 1.05%. This indicated that excessive dosage reduced the effective utilization of the materials. Therefore, 1.0 g L^{-1} of P-nZVI/ESBC composite was selected for the subsequent experiments.

3.2.3. Effect of reaction temperature. The effect of reaction temperatures (15 °C, 25 °C, 35 °C, and 45 °C) on the removal process of TC in aqueous solution were investigated, as shown in Fig. 4C. The removal rate of TC increases with the increasing reaction temperature, showing that the elevated temperature facilitates the removal of TC with P-nZVI/ESBC composites. After 30 min of reaction, the removal rates of TC were 64.6%, 86.5%, 91.0%, and 96.1% at the temperatures of 15 °C, 25 °C, 35 °C, and 45 °C, respectively. The result could be attributed to the fact that the diffusion and mobility of TC molecules in aqueous solution are enhanced at elevated temperature, thus promoting the migration of TC molecules towards P-nZVI/ESBC composite.

3.2.4. Effect of initial pH of TC solution. The solution pH can affect the surface charges of the carbon-based materials and existence forms of TC in aqueous solution.[3,22,38] The effect of initial solution pH on the removal of TC in aqueous solution with P-nZVI/ESBC composites were studied, as shown in Fig. 4D. The removal efficiency of TC first increased and then declined with initial solution pH in the range of 3.0–11.0, and the maximum was found at pH 6.0. When the pH was 3.0, 6.0, 9.0, and 11.0, the corresponding TC removal rates after 240 min of reaction were 90.0%, 98.0%, 66.9%, and 39.1%, respectively.

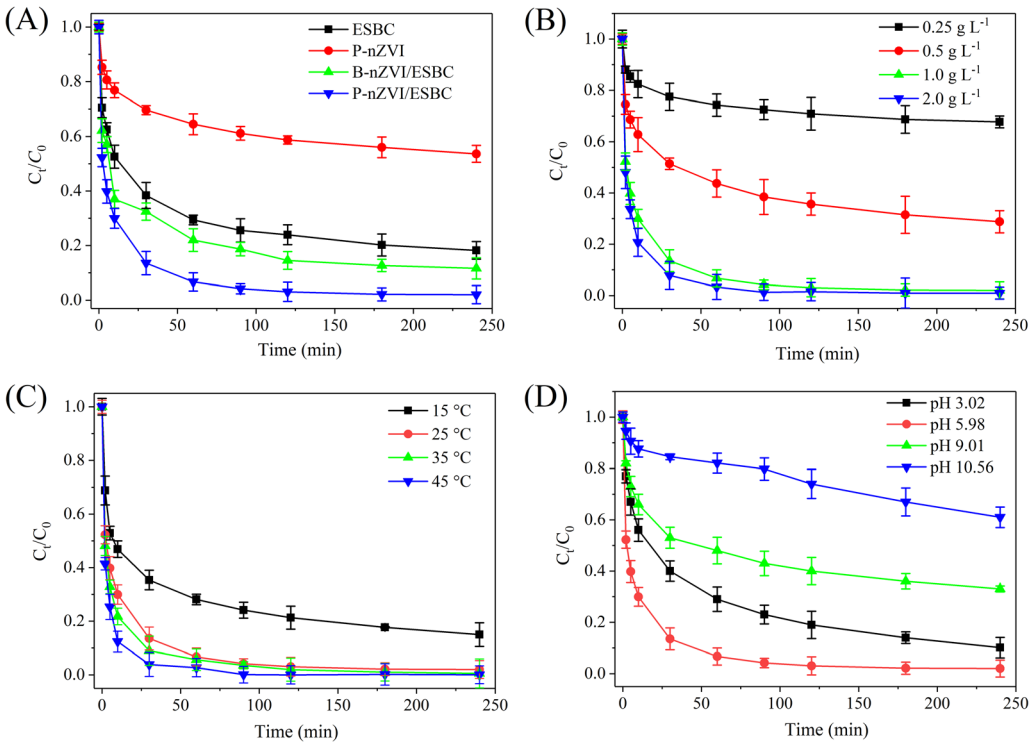

Fig. 4 (A) The removal of TC in aqueous solution with various materials (conditions: material dosage is 1.0 g L^{-1}, initial concentration of TC C_0 is 50 mg L^{-1}, initial pH is 6.0, temperature is 25 °C). (B) The effect of P-nZVI/ESBC composite dosage on TC removal (conditions: C_0 is 50 mg L^{-1}, pH is 6.0, temperature is 25 °C). (C) The effect of reaction temperature on TC removal (conditions: P-nZVI/ESBC dosage is 1.0 g L^{-1}, pH is 6.0, C_0 is 50 mg L^{-1}). (D) The effect of initial pH of TC solution on TC removal (conditions: P-nZVI/ESBC dosage is 1.0 g L^{-1}, C_0 is 50 mg L^{-1}, temperature is 25 °C).

The pH dependence was closely associated with the dissociation state of TC and the charges of the materials in aqueous solution. TC is an amphoteric molecule that exhibits four different predominant species at different pH conditions: H_3TC^+ (cationic, pH < 3.3), H_2TC^0 (zwitterionic, 3.3 < pH < 7.7), HTC^- (anionic 7.7 < pH < 9.7), and TC^- (bivalent anionic pH > 9.7).[3,38] Fig. S4 (ESI)† showed the zeta potential of P-nZVI/ESBC composite at different pH, and the isoelectric point (pH_{iep}) was found approximately 3.6. When the solution pH was 3.0, P-nZVI/ESBC composite was protonated and exhibited positive charges, meanwhile TC in aqueous solution existed mainly as cationic H_3TC^+, thus electrostatic repulsion hindered the transfer of H_3TC^+ to the surface of composite. However, it was worth noting that P-nZVI/ESBC composite still exhibited considerable removal efficiency for TC at pH 3.0, indicating that in addition to electrostatic repulsion, there were additional interactions between TC and the composite,[18,22,38,39] as described in the following TC removal mechanism section. When pH increased to 6.0, the predominant species of TC was zwitterionic H_2TC^0, the low electrostatic repulsion between the composite and TC species resulted in the enhanced TC removal efficiency. As initial pH further increased to 9.0 and 11.0, the predominant species became HTC^- and TC^-, the enhanced electrostatic repulsion can prevent effective contact between the TC species and the composite, resulting in the low removal for TC species. In addition, under strong alkaline conditions, the Fe hydroxide passivation layers tended to form on the surface of composite, which will lead to the decrease in reactivity.

3.3. Adsorption kinetics

Five different adsorption kinetic models including pseudo-first-order (eqn (4)), pseudo-second-order (eqn (5)), Avrami fractional-order (eqn (6)), intra-particle diffusion (eqn (7)), and liquid film diffusion (eqn (8) and (9)) models were used to establish the kinetic predictions for TC adsorption with P-nZVI/ESBC composite. These models are expressed as follows:[2,3,39,40]

$$q_t = q_e(1 - e^{-k_1 t}) \quad (4)$$

$$q_t = \frac{q_e^2 k_2 t}{1 + k_2 q_e t} \quad (5)$$

$$q_t = q_e[1 - e^{-(k_3 t)^n}] \quad (6)$$

$$q_t = k_4 t^{1/2} + C \quad (7)$$

$$\mathrm{Ln}(1 - F) = -k_5 t \quad (8)$$

$$F = \frac{q_t}{q_e} \quad (9)$$

where, k_1 (min^{-1}), k_2 (g mg^{-1} min^{-1}), k_3 (min^{-1}), k_4 (mg g^{-1} min$^{-1/2}$), and k_5 (min^{-1}) represent the adsorption rate constants of pseudo-first-order, pseudo-second-order, Avrami

fractional-order, and intra-particle diffusion models, respectively; C (mg g^{-1}) is the intercept of intra-particle diffusion model; F represents the equilibrium fractional achievement at reaction time t.

The fitted adsorption kinetic curves of P-nZVI/ESBC composite for TC are shown in Fig. 5 and the calculated kinetic parameters are listed in Table 1. According to the fitted results (Table 1), compared to pseudo-first-order model, pseudo-second-order and Avrami fractional-order models are more suitable kinetic models for P-nZVI/ESBC composite in view of the high regression coefficients R^2. This result implied that the adsorption of TC by adsorbent involved multiple kinetic processes and the chemical adsorption may occur.[3,40]

Generally, the adsorption process of contaminants by porous adsorbents can be divided into three stages: mass transfer through external or liquid film diffusion; intra-particle or pore diffusion; adsorption onto active sites of adsorbents.[3] The third stage is usually considered to be fast.[3] In this study, the intra-particle diffusion and liquid film diffusion models were used to further identify the adsorption mechanism and rate-determining step of adsorption reaction.[3,40,41] As shown in Fig. 5B, the plots of q_t *vs.* $t^{1/2}$ exhibit multi-linear regions with three slopes for P-nZVI/ESBC composite. The low R^2 values (0.7410 and 0.6439) of fitted intra-particle diffusion models and no straight lines derived from the slopes pass through the origin, suggesting that the adsorption process of TC may not be controlled by intra-particle diffusion.[38,41] Moreover, the large intercepts (28.73 and 147.10) indicate that the adsorption may occur on the surfaces of adsorbents.[3] From Fig. 5C, it is observed that the liquid film diffusion model can well fit the experimental data of P-nZVI/ESBC composites for TC adsorption. The high R^2 values (0.9891 and 0.9370) and small intercepts (0.8980 and 0.9680) suggest that liquid film diffusion may be the rate-determining step for TC adsorption onto the adsorbents.[3] In summary, the adsorption of TC by P-nZVI/ESBC composite involved multiple kinetic processes and the chemisorption may occur, liquid film diffusion rather than internal particle diffusion was the adsorption rate-determining step.

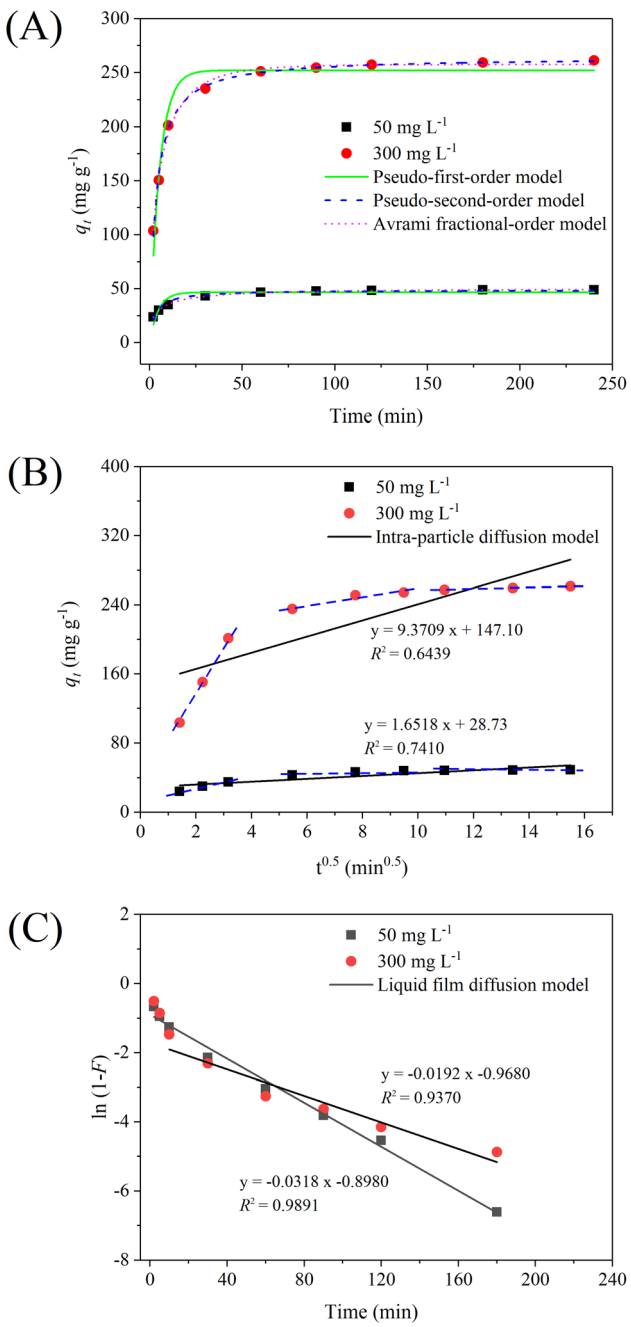

Fig. 5 (A) Pseudo-first-order, pseudo-second-order, and Avrami fractional-order, (B) intra-particle diffusion, and (C) liquid film diffusion models for TC removal with P-nZVI/ESBC composite. (Conditions: material dosage is 1.0 g L^{-1}, C_0 are 50 mg L^{-1} and 300 mg L^{-1}, pH is 6.0, temperature is 25 °C).

3.4. Adsorption isotherms

In this work, to further study the adsorption behavior of P-nZVI/ESBC composite for TC, batch adsorption experiments were performed at initial TC concentrations from 50 to 400 mg L^{-1}. Three well-known adsorption isotherm models including Langmuir (eqn (10) and (11)), Freundlich (eqn (12)) as well as Sips (eqn (13)) models were used to match the experimental data, respectively.

$$q_e = \frac{q_m k_L C_e}{1 + k_L C_e} \quad (10)$$

$$R_L = \frac{1}{1 + k_L C_0} \quad (11)$$

$$q_e = k_F C_e^{\frac{1}{n}} \quad (12)$$

$$q_e = \frac{q_m (k_S C_e)^m}{1 + (k_S C_e)^m} \quad (13)$$

where, Langmuir model: the k_L (L mg^{-1}) represents the Langmuir constant associated with the adsorption energy; R_L is the separation factor and its value shows that the adsorption isotherm is irreversible ($R_L = 0$), favorable ($0 < R_L < 1$), linear ($R_L = 1$), and unfavorable ($R_L > 1$).[3,18] Freundlich model: k_F (mg g^{-1} (L mg^{-1})$^{1/n}$) and $1/n$ stand for the constants of Freundlich

Table 1 The adsorption kinetic parameters of TC with P-nZVI/ESBC composite

	Pseudo-first-order model			Pseudo-second-order model			Avrami fractional-order model			
	k_1 (min^{-1})	q_e (mg g^{-1})	R^2	k_2 (g mg^{-1} min^{-1})	q_e (mg g^{-1})	R^2	k_3 (min^{-1})	q_e (mg g^{-1})	n	R^2
50 mg g^{-1}	0.2212	46.69	0.8042	0.0073	48.78	0.9555	0.2241	47.97	0.5156	0.9928
300 mg g^{-1}	0.1921	252.98	0.9477	0.0011	264.22	0.9954	0.1824	259.05	0.5341	0.9932

model associated with the adsorption capacity and adsorption intensity or the heterogeneity of the adsorbent, respectively; $1/n$ shows that the adsorption isotherm is undesirable ($1/n > 1$), desirable ($0 < 1/n < 1$), and irreversible ($1/n < 0$).[3] Sips model: k_S (L mg^{-1}) and m are the factors of Sips model related to the adsorption capacity and the heterogeneity of the adsorbent materials, respectively.

The fitted results of experimental data and corresponding parameters of adsorption isotherm models are shown in Fig. 6 and Table 2. The Langmuir model is a theoretical model based on the homogeneous surface adsorption and assumes the adsorption in monomolecular layer.[3,42] The Freundlich model is an empirical equation that multilayer adsorption occurs on heterogeneous surface.[3,42] As shown in Table 2, it is evident that the Langmuir and Freundlich models can match the experimental data well in view of the high correlation coefficients (both $R^2 > 0.95$). The result indicated that the adsorption of TC on P-nZVI/ESBC composite was not a rigorous monomolecular layer adsorption on the homogeneous surface, and the multilayer adsorption also existed on heterogeneous surface, especially at high TC concentration.[38,39,43] This conclusion was further confirmed by the fitted results of Sips model. Sips model is the combination of Langmuir and Freundlich models. Compared with Langmuir and Freundlich models, Sips model had the highest correlation coefficients R^2 of 0.9961 (Table 2), indicating that the adsorption of TC on the adsorbents involved multiple mechanisms. In addition, the maximum adsorption capacity of P-nZVI/ESBC composite for TC was up to 304.62 mg g^{-1} (seen Fig. 6), which was superior to most other adsorbents reported in previous literature (Table S2, ESI†). The values of Langmuir factor R_L and Freundlich factor $1/n$ were 0.0208 ($0 < R_L < 1$) and 0.3076 ($0 < 1/n < 1$), respectively, implying that the adsorption process of TC on P-nZVI/ESBC composite was favorable.[3]

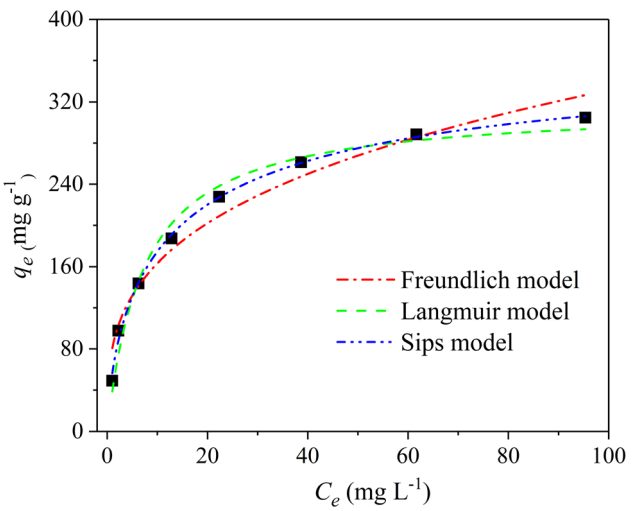

Fig. 6 The adsorption isotherms of TC with P-nZVI/ESBC composite. (Conditions: material dosage is 1.0 g L^{-1}, C_0 are 50–400 mg L^{-1}, pH is 6.0, temperature is 25 °C).

3.5. Reusability of material

Reusability is an important indicator for evaluating the practical application of adsorbents, which is related to the cost of use and the environmental safety of adsorbents. Therefore, the adsorption–desorption cycle experiments were carried out to estimate the reusability of material. As shown in Fig. S5 (ESI),† P-nZVI/ESBC composite maintained a stable removal performance for TC. After five adsorption–desorption cycles, the removal rate of TC still reached 68.2% with 240 min. This result implies that green synthesized P-nZVI/ESBC composite has good reusability and stability, and shows a promising application prospect in antibiotic wastewater treatment.

3.6. Possible removal mechanism for TC

In this study, in order to analyze the possible removal mechanism of TC by P-nZVI/ESBC composite, the variation of residual TOC in the filtrate was measured during the reaction, and the results are shown in Fig. 7A. It was generally accepted that if TC in aqueous solution was only degraded to smaller organic products and not be adsorbed, the residual TOC in the filtrate should remained constant and TC concentration should decrease.[11,22] In Fig. 7A, the decrease of residual TOC in the filtrate illustrated that adsorption mechanism was participated in the removal of TC. Based on the characterization results in the Section 3.1, P-nZVI/ESBC composites are porous structures and contain numerous oxygen-containing functional groups (such as hydroxyl, carbonyl, and carboxyl groups), implying that they can adsorb TC species in aqueous solution through hydrogen bonding,[1] π–π electron donor–acceptor (π–π EDA) interactions,[1,3] and pore filling effect.[18] In addition, according to the results of XPS, P-nZVI/ESBC composite surfaces possess Fe(III) species, which may interact with amide groups on TC to form Fe(III)–TC complexes.[22,44] The adsorption kinetic model analyses (Section 3.3) also showed that the adsorption of TC by P-nZVI/ESBC composite involved multiple kinetic processes and chemisorption may occur. In addition, as shown in Fig. 7A, 98.0% of TC in the solution was removed within 240 min, while TOC decrement was 82.6%. The result suggests that in addition to the adsorption, the reductive degradation of TC by P-nZVI/

Table 2 The adsorption isotherm parameters of TC with P-nZVI/ESBC composite

Models	Parameter 1	Parameter 2	Parameter 3	R^2
Langmuir	$q_m = 315.92$ mg g^{-1}	$k_L = 0.1372$ L mg^{-1}	$R_L = 0.0208$	0.9777
Freundlich	$k_F = 80.37$ (mg g^{-1} (L mg^{-1})$^{1/n}$)	$1/n = 0.3076$		0.9571
Sips	$q_m = 383.89$ mg g^{-1}	$k_S = 0.0767$ L mg^{-1}	$m = 0.6893$	0.9961

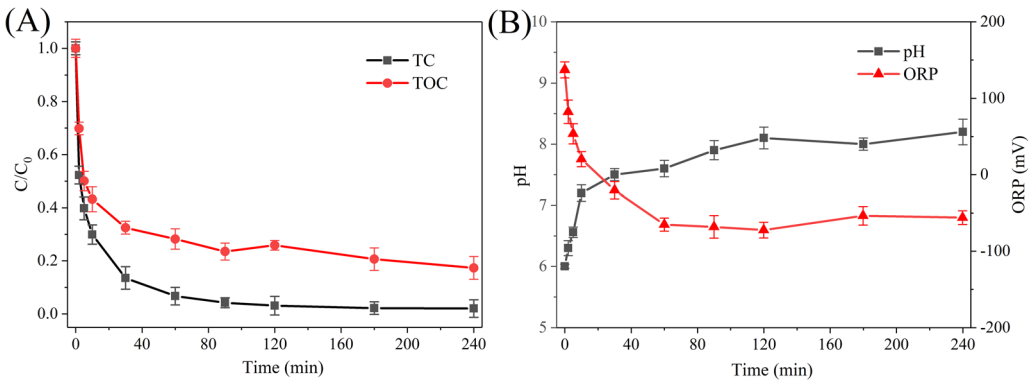

Fig. 7 The variations of TC and TOC (A) and pH and ORP (B) in aqueous solution during the reaction between P-nZVI/ESBC composite and TC. (Conditions: material dosage is 1.0 g L^{-1}, C_0 is 50 mg L^{-1}, pH is 6.0, temperature is 25 °C).

ESBC composite may play a role in the reaction. The degradation products of TC could be analyzed qualitatively using LC-MS. During the reaction, three degradation products with m/z of 270.9, 329.5 and 387.1 in the filtrate were observed, as shown in Table S3 (ESI).† The similar results were also reported in previous studies where PVP–nZVI and CS–nZVI nanoparticles were used to degrade TC.[22,45] However, it was noteworthy that our results were different from that of Dong *et al.*,[5] in which TC was degrade with Ni/Fe bimetallic nanoparticles. The differences in TC degradation products distribution may be attributed to the involvement of different reaction mechanism. In Ni–Fe bimetallic system, Ni can adsorb H_2 generated from Fe^0 corrosion and activate H_2 to form H* species, H-transfer may be the dominant degradation mechanism.[5,46] While, in this study, the transfer of electrons originating from Fe^0 corrosion might be responsible for the reductive degradation of TC.

To further elaborate the degradation mechanism for TC, the differences in chemical compositions of P-nZVI/ESBC composite surfaces before and after reaction with TC were analyzed by XPS, as shown in Fig. 3B and S6 (ESI).† After reaction with TC, typical Fe^0 peak at around 706.4 eV significantly decreased (Fig. S6†), implying the consumption of Fe^0 due to the TC reductive degradation process. In addition, compared to fresh P-nZVI/ESBC composite (Fig. 3B), the intensity corresponding to Fe–O in O 1s XPS spectra (Fig. S7, ESI†) increased from 24.8% to 30.3% after reaction with TC, further indicating the formation of new iron oxides. The variations of pH and ORP in the solution during the reaction also indicated that the consumption of Fe^0 may be involved in the reductive degradation for TC, as shown in Fig. 7B. During the reaction, solution pH increased from 6.0 to the equilibrium of about 8.2, which was attributed to the consumption of H^+ (eqn (14)) and the generation of OH^- (eqn (15)). In addition, the solution ORP decreased from 170.2 mV to −56 mV after 240 min of reaction, which was attributed to the generation of reducing species (Fe^{2+} and H_2) (eqn (14) and (15)) during the reaction. The strong reducing atmosphere was favorable for the reductive degradation of TC.

$$Fe^0 + 2H^+ \rightarrow Fe^{2+} + H_2\uparrow \text{ (acidic condition)} \quad (14)$$

$$Fe^0 + 2H_2O \rightarrow Fe^{2+} + H_2\uparrow + 2OH^- \text{ (neutral or alkaline conditions)} \quad (15)$$

Overall, the possible mechanisms of TC removal by P-nZVI/ESBC composite may include the following aspects: (i) the bulk of TCs were adsorbed by P-nZVI/ESBC composite involving hydrogen bonding,[1] π–π EDA interactions,[1,3] pore filling effect, and Fe(III)–TC complexation, and the liquid film diffusion may be the rate-limiting step; (ii) the partial TCs may be reductively degraded *via* electron transfer mechanism.

4. Conclusion

In this work, a novel P-nZVI/ESBC composite was successfully synthesized using pomegranate peel extract as the green reducing agent and NaOH modified eggplant straw biochar (ESBC) as the carrier. Compared to other prepared materials, P-nZVI/ESBC composite exhibited excellent removal performance for TC (304.62 mg g^{-1}, 25 °C). Reaction temperature and solution pH played the important roles for TC removal. The adsorption of TC by P-nZVI/ESBC composite involved multiple kinetic processes and the chemical adsorption may occur. The hydrogen bonding, π–π EDA interactions, pore filling, Fe(III)–TC complexation, and reductive degradation were the dominant

mechanisms for TC removal. This study shows that P-nZVI/ESBC composite can be used as the low-price and effective adsorbent material in antibiotics remediation field.

Data availability

All relevant data are included in the paper or its ESI.†

Author contributions

Guofu Huang, Mianmian Wang, and Fangfang Liu: experimental design, data curation, writing original draft and funding. Qing Liu, and Shasha Zhao: draft revision. Haijian Liu and Jun Liu: experiment and data collection. All authors read and approved the final manuscript.

Conflicts of interest

The authors declare there is no conflict.

Acknowledgements

This work was supported by the Weifang University of Science and Technology Fund (2021XKJS39, 2022KJ06), the Project of Weifang Science and Technology Development Plan (2021GX048, 2022GX038), Nature Science Foundation of Shandong Province (ZR2022MB118), the Innovation Capacity Enhancement Project of Science and Technology-based Small and Medium-sized Enterprises (2023TS1005, 2023TSGC0736), Shandong Student Innovation and Entrepreneurship Training Program (S202312843065).

References

1 H. Wang, C. Fang, Q. Wang, Y. Chu, Y. Song, Y. Chen and X. Xue, *RSC Adv.*, 2018, **8**, 16260–16268.
2 J. Shi, X. Yang, C. Zhang, X. Feng, X. Kong, X. Wang and S. Wang, *Environ. Pollut. Bioavailability*, 2021, **33**, 247–254.
3 Y. Zhou, X. Liu, Y. Xiang, P. Wang, J. Zhang, F. Zhang, J. Wei, L. Luo, M. Lei and L. Tang, *Bioresour. Technol.*, 2017, **245**, 266–273.
4 X. Wu, Y. Wei, J. Zheng, X. Zhao and W. Zhong, *Bioresour. Technol.*, 2011, **102**, 5924–5931.
5 H. Dong, Z. Jiang, C. Zhang, J. Deng, K. Hou, Y. Cheng, L. Zhang and G. Zeng, *J. Colloid Interface Sci.*, 2018, **513**, 117–125.
6 F. Akram, M. Imtiaz and I. ul Haq, *Microb. Pathog.*, 2022, 105923.
7 S. Li, B. S. Ondon, S.-H. Ho and F. Li, *Environ. Res.*, 2022, 115132.
8 H. Huang, Z. Niu, R. Shi, J. Tang, L. Lv, J. Wang and Y. Fan, *Bioresour. Technol.*, 2020, **306**, 123096.
9 J. Guo, M. Huang, P. Gao, Y. Zhang, H. Chen, S. Zheng, T. Mu and X. Luo, *Chem. Eng. J.*, 2020, **398**, 125604.
10 X. Chen, Y. Yang, Y. Ke, C. Chen and S. Xie, *Sci. Total Environ.*, 2022, **814**, 152852.
11 G. Gopal, H. Sankar, C. Natarajan and A. Mukherjee, *J. Environ. Manage.*, 2020, **254**, 109812.
12 Y. Shi, J. Li, D. Wan, J. Huang and Y. Liu, *Sci. Total Environ.*, 2020, **749**, 142313.
13 Y. Cao, L. Yue, Z. Li, Y. Han, J. Lian, H. Qin and S. He, *Appl. Surf. Sci.*, 2023, **609**, 155191.
14 T. Li, F. Zhu, W. Liang, G. Hu, X. Deng, Y. Xue and J. Guan, *Process Saf. Environ. Prot.*, 2022, **167**, 629–640.
15 Y. Cai, J. Fan and Z. Liu, *J. Hazard. Mater.*, 2022, **436**, 129092.
16 X. Wang, Y. Zhuang, J. Zhang, L. Song and B. Shi, *Sci. Total Environ.*, 2020, **714**, 136436.
17 S.-Q. Chen, Y.-L. Chen and H. Jiang, *Ind. Eng. Chem. Res.*, 2017, **56**, 3059–3066.
18 H. Liu, G. Xu and G. Li, *J. Colloid Interface Sci.*, 2021, **587**, 271–278.
19 X. Jian, X. Zhuang, B. Li, X. Xu, Z. Wei, Y. Song and E. Jiang, *Environ. Technol. Innov.*, 2018, **10**, 27–35.
20 C. Liu, X. Huang and L. Kong, *Energies*, 2017, **10**, 2094.
21 G. Gascó, J. Paz-Ferreiro, M. L. Álvarez, A. Saa and A. Méndez, *Waste Manage.*, 2018, **79**, 395–403.
22 H. Chen, H. Luo, Y. Lan, T. Dong, B. Hu and Y. Wang, *J. Hazard. Mater.*, 2011, **192**, 44–53.
23 H. Tang, J. Wang, S. Zhang, H. Pang, X. Wang, Z. Chen, M. Li, G. Song, M. Qiu and S. Yu, *J. Clean. Prod.*, 2021, **319**, 128641.
24 H. Wu, W. Wei, C. Xu, Y. Meng, W. Bai, W. Yang and A. Lin, *Ecotoxicol. Environ. Saf.*, 2020, **188**, 109902.
25 G. M. Yıldırım and B. Bayrak, *Biomass Convers. Biorefin.*, 2021, 1–13.
26 T. Wang, X. Jin, Z. Chen, M. Megharaj and R. Naidu, *Sci. Total Environ.*, 2014, **466**, 210–213.
27 X. Weng, L. Huang, Z. Chen, M. Megharaj and R. Naidu, *Ind. Crop. Prod.*, 2013, **51**, 342–347.
28 Y. Wei, Z. Fang, L. Zheng, L. Tan and E. P. Tsang, *Mater. Lett.*, 2016, **185**, 384–386.
29 Z. Xiao, M. Yuan, B. Yang, Z. Liu, J. Huang and D. Sun, *Chemosphere*, 2016, **150**, 357–364.
30 L. Yang, J. Shen, W. Zhang, W. Wu, Z. Wei, M. Chen, J. Yan, L. Qian, L. Han and J. Li, *Sci. Total Environ.*, 2022, **829**, 154645.
31 Y. Zhang, X. Jiao, N. Liu, J. Lv and Y. Yang, *Chemosphere*, 2020, **245**, 125542.
32 X. Wang, A. Wang, J. Ma and M. Fu, *Chemosphere*, 2017, **166**, 80–88.
33 P. Dauthal and M. Mukhopadhyay, *J. Ind. Eng. Chem.*, 2015, **22**, 185–191.
34 Z. Pan, Y. Lin, B. Sarkar, G. Owens and Z. Chen, *J. Colloid Interface Sci.*, 2020, **558**, 106–114.
35 Y. Xin, P. Zhang, J. Shen and S. Ren, *Water*, 2022, **14**, 2734.
36 X. Dai, H. Fan, C. Yi, B. Dong and S. Yuan, *J. Mater. Chem. A*, 2019, **7**, 6849–6858.
37 H. Wu, Q. Feng, H. Yang, P. Lu, B. Gao and A. Alansari, *Environ. Technol.*, 2018, **40**, 3114–3123.
38 X. Wang, W. Lian, X. Sun, J. Ma and P. Ning, *Front. Environ. Sci. Eng.*, 2018, **12**, 1–11.
39 U. A. Guler, *J. Environ. Eng. Landsc. Manag.*, 2017, **25**, 223–233.

40 J. Qu, Y. Liu, L. Cheng, Z. Jiang, G. Zhang, F. Deng, L. Wang, W. Han and Y. Zhang, *J. Hazard. Mater.*, 2021, **403**, 123607.
41 T. Wang, L. Zhang, C. Li, W. Yang, T. Song, C. Tang, Y. Meng, S. Dai, H. Wang and L. Chai, *Environ. Sci. Technol.*, 2015, **49**, 5654–5662.
42 J. Ma, B. Zhou, H. Zhang, W. Zhang and Z. Wang, *Chem. Eng. Res. Des.*, 2019, **149**, 209–219.
43 J. Tang, Y. Huang, Y. Gong, H. Lyu, Q. Wang and J. Ma, *J. Hazard. Mater.*, 2016, **316**, 151–158.
44 L. Peng, Y. Ren, J. Gu, P. Qin, Q. Zeng, J. Shao, M. Lei and L. Chai, *Environ. Sci. Pollut. Res.*, 2014, **21**, 7631–7640.
45 X. Wang, B. Zhang, J. Ma and P. Ning, *Environ. Eng. Sci.*, 2019, **36**, 273–282.
46 Y. Li, X. Li, D. Han, W. Huang and C. Yang, *Chem. Eng. J.*, 2017, **311**, 173–182.